RESILIENT INFRASTRUCTURE
June 1–4, 2016
RESILIENT INFRASTRUCTURE LONDON 2016

COVER CRACK GROWTH MONITORING IN RC STRUCTURES SUBJECTED TO CORROSION WITH ACOUSTIC EMISSION SENSORS

Ahmed A. Abouhussien
Memorial University of Newfoundland, Canada

Assem A. A. Hassan
Memorial University of Newfoundland, Canada

ABSTRACT

This paper investigates the feasibility of applying acoustic emission (AE) monitoring to evaluate the cover cracking caused by reinforcing steel corrosion in concrete structures. Ten small-scale reinforced concrete prism samples were continuously monitored using attached AE sensors as being exposed to accelerated corrosion tests. The samples had a constant concrete cover (40 mm) around one embedded steel bar and were corroded to reach five percentages of steel mass loss: 1%, 2%, 3%, 4%, and 5%. Several AE signal parameters including number of hits, signal strength, energy, amplitude, and peak frequency were acquired during the tests. The AE signal strength data were also incorporated in an intensity analysis to attain two additional AE parameters namely; historic index ($H(t)$) and severity (S_r). For the comparison, visual inspection of all samples was performed to detect and measure cover crack widths. The results indicated that AE parameters especially $H(t)$ and S_r were in a good correlation with the corresponding values of crack widths at all percentages of steel mass loss. In addition, a damage classification chart was generated using the values of $H(t)$ and S_r to predict the cover crack width associated with reinforcement corrosion in concrete structures.

Keywords: structural health monitoring; acoustic emission sensors; crack growth; reinforcing steel corrosion; signal strength; concrete structures.

1. INTRODUCTION

Corrosion of reinforcing steel is considered one of the major causes of deterioration of concrete structures, which affects serviceability and overall service lifetime. The concrete cover protects the embedded steel from premature corrosion due to the natural alkaline environment of the surrounding concrete. However, when concrete structures are exposed to chlorides from different sources, chlorides can penetrate the concrete cover, decrease the concrete alkalinity, and attack the embedded steel. The increased concentration of the chlorides around the reinforcing steel leads to corrosion initiation. This is followed by corrosion propagation and accumulation of corrosion products around the reinforcing steel surface. Corrosion products, with its larger volume, lead to the expansion of steel bars and eventually to concrete cover cracking. This concrete cover cracking can directly expose the reinforcing steel to higher chloride exposure and consequently lead to significantly higher corrosion rate (Otieno et al. 2010, Di Benedetti et al. 2013).

Different nondestructive testing (NDT) techniques were successfully applied to identify and evaluate potential deterioration in concrete structures. However, most of these methods are intrusive and require regular site visits for efficient condition assessment. Instead, continuous structural health monitoring (SHM) systems are recently being applied for both damage prognosis and diagnosis of concrete structures. Acoustic emission (AE) sensors are used as a strong tool for testing and evaluating the behaviour of materials and structures deforming under stresses. AE sensors have successfully been implemented in SHM systems for condition assessment and long-term monitoring of civil infrastructure systems. This type of monitoring showed great potential for early detection of different forms of deteriorations in reinforced concrete structures (Nair and Cai 2010, ElBatanouny et al. 2014). AE sensors can be

exploited in SHM systems to measure a variety of signal parameters that can be analyzed to detect and evaluate the level of damage that follows corrosion of steel in reinforced concrete.

AE technique has extensively been applied to monitor corrosion in reinforced concrete structures. A number of experimental investigations (Li et al. 1998, Ohtsu and Tomoda 2008, Di Benedetti et al. 2013, Kawasaki et al. 2014) have examined the feasibility of using attached AE sensors to detect corrosion of steel in small-scale reinforced concrete samples. The outcomes from these experimental studies show that different AE signal parameters can be analyzed to achieve early corrosion detection when compared to traditional NDT methods. The application of AE has also been extended to detecting corrosion of prestressed concrete small-scale samples (Ramadan et al. 2008, Mangual et al. 2013). The results obtained from these investigations showed the possibility of using AE signal parameters to characterize and quantify the extent of damage in prestressed concrete structures. The applications of AE have also been confirmed by testing larger-scale samples, including prestressed concrete girders and piles (ElBatanouny et al. 2014, Vélez et al. 2015).

AE intensity analysis is an analysis that can be performed on AE signal strength to obtain parameters that characterize the level of damage of structures. This analysis was first applied in fibre-reinforced polymer (FRP) vessels and has further been adopted in the literature to characterize damage in prestressed concrete structures (Mangual et al. 2013, ElBatanouny et al. 2014, Vélez et al. 2015). The outcomes of this analysis can be utilized to develop damage classification charts based on the collected AE signal strength. However, further research is needed to apply the AE intensity analysis to quantify cover cracking in concrete structures considering the effects of the degree of steel corrosion. The objective of this study was to apply the AE intensity analysis to evaluate the extent of damage of the concrete cover in reinforced concrete prone to corrosion of reinforcing steel. In addition, the aim was to investigate the effect of the severity of corrosion damage (in terms of higher degrees of steel mass loss) on different AE signal parameters.

2. EXPERIMENTAL PROGRAM

Ten small-scale reinforced concrete prism samples were subjected to an accelerated corrosion test and the rate of corrosion was continuously monitored using AE sensors (Figure 1). These prism samples were constructed with constant concrete covers (40 mm) around one embedded steel bar at the centre of each prism. The dimensions of all prism samples were 100 x 100 x 250 mm. All samples were cured in water for a period of 28 days before the corrosion exposure. The samples were exposed to corrosion using an impressed current accelerated corrosion test until reaching variable levels of damage. These different degrees of damage were estimated based on the theoretical mass loss of steel, including 1%, 2%, 3%, 4%, and 5%. Two identical samples were tested at each degree of mass loss to confirm the repeatability of the test results. The selected levels of mass loss were presumed, based on reviewing the literature, to obtain the range of the critical corrosion degree that causes cover cracking in reinforced concrete structures. This literature review showed that a critical range of 0.8% to 5.6% of steel mass loss may induce cover cracking with cover thickness ranges between 10 mm and 50 mm (Oh et al. 2009). The targeted values of the theoretical mass loss of steel in all tested samples were calculated by applying Faraday's law (Eq. 1).

$$\text{Mass loss} = \frac{t \,.\, i \,.\, M}{z \,.\, F} \quad [1]$$

Where: t = the time passed (s); i = the current passed (Ampere); M = atomic weight (for steel: M = 55.847 g/mol); z = ion charge (2 moles of electrons); and F = Faraday's constant, which is the amount of electrical charge in one mole of an electron (F = 96485 coulombs per mole (C/mol)).

The tested samples were designated according to the percentage of steel mass loss (1%, 2%, 3%, 4%, and 5%), and replicate number (1 or 2). For instance, the first replicate of the prism sample exposed to 3% steel mass loss is identified as S3-1.

2.1 Mixture Proportions and Material Properties

The concrete mixture used in this paper contained type GU Canadian Portland cement, similar to ASTM Type I (ASTM C150), with a specific gravity of 3.15. Natural sand and 10 mm maximum size stone were incorporated into

the mixture as fine and coarse aggregates, respectively. Both coarse and fine aggregates had a specific gravity of 2.60 and water absorption of 1%. The 28-day compressive strength of concrete was obtained by testing six 100-mm diameter x 200-mm high cylindrical samples according to ASTM C39. The compressive strength of the concrete mixture used herein indicated an average of 33.47 MPa with a standard deviation of 0.8 MPa, as seen in Table 1. Carbon steel bars with a 20 mm diameter were used in all of the tested prism samples. All reinforcing steel bars have an average yield stress of 480 MPa and an average tensile strength of 725 MPa. The mixture properties and 28-day compressive strength results of the concrete mixture are shown in Table 1.

Table 1: Mixture design and 28-day compressive strength for the concrete mixture

Cement (kg/m^3)	10 mm stone (kg/m^3)	Sand (kg/m^3)	Water (kg/m^3)	28-day compressive strength (MPa)
350	1168.27	778.84	140	$f_c' = 33.47 \pm 0.8$

2.2 Accelerated Corrosion Test Procedure

All tested samples were subjected to an electrically accelerated corrosion test, as shown in Figure 1. A constant voltage (12 Volts) was applied to all tested samples during the test. The prism samples were partially submerged in a plastic container filled with a 5% NaCl water solution. The embedded steel bar in each sample was connected as an anode (+) in a DC power supply, whereas a stainless steel mesh was placed underneath all samples to act as a cathode (–). The amount of the electric current passing in each sample was constantly monitored and recorded at one-minute intervals using a data-acquisition system. Based on the recorded values of the electric current and passed time, the predicted percentage of steel mass loss was calculated using Eq. 1 until the target values were reached. The samples were also visually inspected on a daily basis to detect the concrete cover cracking and to measure the crack widths by means of a crack-width-measuring microscope. The test was ended for each sample after reaching the previously assumed degrees of steel mass loss (1 to 5%). The percentage of steel mass loss was verified at the end of the test by breaking the samples and weighing the steel bar to obtain the actual mass loss, as per ASTM G1.

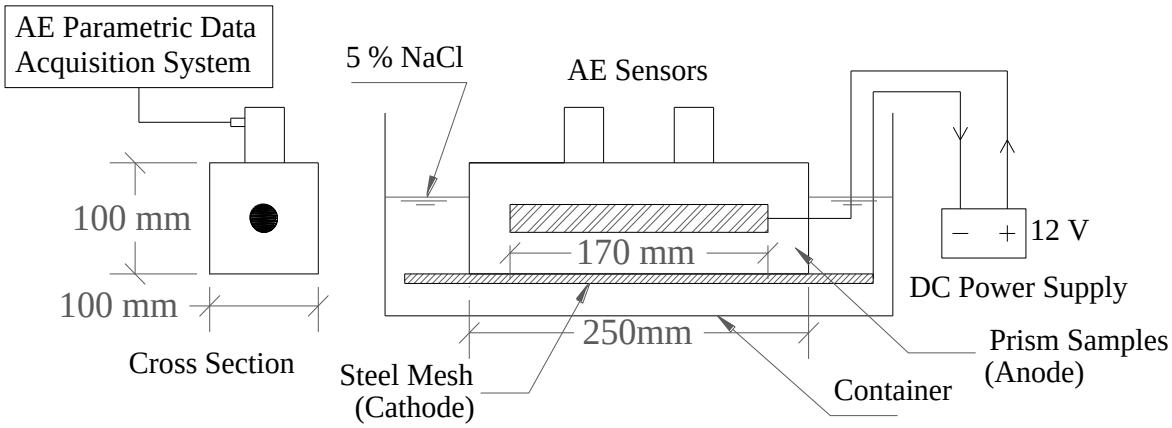

Figure 1: Accelerated corrosion and AE monitoring test setup

2.3 Acoustic Emission Monitoring

The acoustic emissions, resulting from the steel corrosion in each sample during the accelerated corrosion test, were monitored using two piezoelectric AE sensors with integral preamplifier (Physical Acoustics 2005). These sensors were attached at the top of each sample's surface using a two-part epoxy adhesive (an epoxy resin and a hardener) on the centre of the steel bar, as seen in Figure 1. The generated acoustic emissions were continuously acquired and recorded using a 4-channel AE data acquisition system and AEwin signal processing software (Mistras Group 2007). An amplitude threshold value of 40 dB was utilized to record AE signals using the data acquisition system. The AE hardware was set up to gather variable AE signal parameters including amplitude, energy, duration, signal strength, absolute energy, and peak frequency. The definition of different AE signal parameters and other terminology for nondestructive testing are available elsewhere (ASTM E1316). These different signal parameters

can be evaluated to characterize and quantify the level of damage arising from any deterioration in concrete structures. These parameters were selected based on reviewing the most significant AE parameters for characterizing corrosion in concrete structures (For example: Li et al. 1998, Di Benedetti et al. 2013, Mangual et al. 2013, ElBatanouny et al. 2014, Kawasaki et al. 2014).

3. RESULTS AND DISCUSSIONS

The results obtained at the end of the accelerated corrosion test on all tested samples are shown in Table 2. These results include the test duration, time to detect cover cracking by visual inspection, both theoretical and actual percentages of steel mass loss, and crack widths at the end of the experiment. The table also shows that the actual degrees of steel mass loss were mostly in good agreement with the predicted percentage of steel mass loss results. All tested samples showed a typical cracking behaviour, as seen from the example in Figure 2. It can be noticed from the figure that the sample, exhibited one crack along the length of the embedded bar on only one side of the specimen. The results in Table 2 will be used as a benchmark for the results obtained from AE monitoring in order to characterize the damage in the cover zone in terms of AE data.

Table 2: Results of all tested samples at the end of the accelerated corrosion test

Specimen	Test duration (days)	Theoretical mass loss of steel (%)	Actual mass loss of steel (%)	Time to first crack (days)	Final crack width (mm)
S1-1	12	1	0.9	10	0.1
S1-2	12	1	0.8	10	0.08
S2-1	15	2	1.8	10	0.46
S2-2	15	2	1.8	10	0.48
S3-1	17	3	3.0	10	0.72
S3-2	17	3	2.8	10	0.8
S4-1	19	4	3.9	10	1.12
S4-2	19	4	4.0	10	1.23
S5-1	21	5	4.8	10	1.88
S5-2	21	5	4.9	10	1.95

Figure 2: Typical cracking behaviour of tested samples

3.1 Acoustic Emission Data Filtering

At the end of each test, the acquired AE results were filtered to reduce any signals related to noise or unwanted wave reflections recorded during the test. For this reason, an amplitude-duration-based filter or Swansong II filter was applied here. This filtering approach has successfully been performed in similar experimental studies (ElBatanouny et al. 2014, Vélez et al. 2015). In this approach, all signals that exhibited both higher amplitudes and relatively long durations were rejected according to the presented ranges of amplitude-duration in Table 3. Furthermore, all signals that exhibited low amplitude values from 40 to 45 dB were attributed to noise and thus were all filtered. After performing the previously mentioned filtering process, the remaining AE data were deemed actual emissions resulting from corrosion propagation and cover cracking in all tested samples. These data were subjected to further analysis and are discussed in the following sections.

Table 3: Rejection limits for amplitude-duration-based filter (Vélez et al. 2015)

Amplitude range (dB)	Duration (μs)	
	Lower	Upper
40<A<45*	—	—
45 ≤ A<54	0	1000
54 ≤ A<60	100	1000
60 ≤ A<65	300	1000
A ≥ 65	500	1000

* All signals were rejected regardless of the duration value

3.2 Effect of Cover Crack Growth on Different Acoustic Emission Parameters

The results in Table 2 show that all tested samples exhibited an overall increase in the values of crack width with higher levels of corrosion (higher percentages of steel mass loss). Figures 3 to 5 show the impact of the increase in crack widths on different AE parameters in a typical sample corroded up to 3% of steel mass loss (S3-1), as an example. The figures show the variations of the number of hits (Figure 3), cumulative signal strength (CSS) (Figure 4), and cumulative energy (CE) (Figure 5) versus test time. It can be realized from the figures that the increase in crack width as a result of corrosion showed an overall increase in the results of number of hits, CSS, and CE. These figures, however, demonstrated an increase in number of hits, CSS, and CE before the detection of the first visual crack in this sample. This increase may be related to the movement of chlorides through the sample and further to the depassivation of steel and corrosion initiation. It is also clear that these graphs exhibited sudden increases at certain times of the test in all tested covers. For instance, the CSS versus time curve for S3-1 (Figure 4) has two points of sudden activity at nearly 120 hr and 205 hr. The first sudden change, at about 120 hr, is mostly related to the onset of steel corrosion, which also showed a significant increase in the number of hits and CE (Figures 3 and 5). The second point, at almost 205 hr, can be correlated to the inception of micro-cracking resulting from the rebar expansions, which is due to the accumulation of corrosion products. This increased AE activity was further confirmed by the detection of the first visual crack (width of 0.08 mm) in this sample (S3-1) at 240 hr (Table 2). After these two points of the curve, the results of number of hits, CSS, and CE showed an almost linear increasing trend, indicating further opening of the crack. These detections of sudden changes in number of hits, CSS, and CE curves were used by other researchers to indicate different stages of corrosion of steel in concrete structures (Di Benedetti et al. 2013, Mangual et al. 2013, ElBatanouny et al. 2014, Vélez et al. 2015).

The results of number of hits, CSS, and CE at the end of the test for all other tested samples are summarized in Table 3. The results presented in Table 3 also confirm that increasing cover crack widths (higher percentages of steel mass loss) yielded higher number of hits, CSS, and CE in all tested specimens. Although these relationships can give an indication of the crack growth by this continuously increasing trend of AE activity, it cannot be applied to quantify the amount of crack width. Instead, an intensity analysis should be performed to assess the extent of cover cracking due to corrosion of embedded steel.

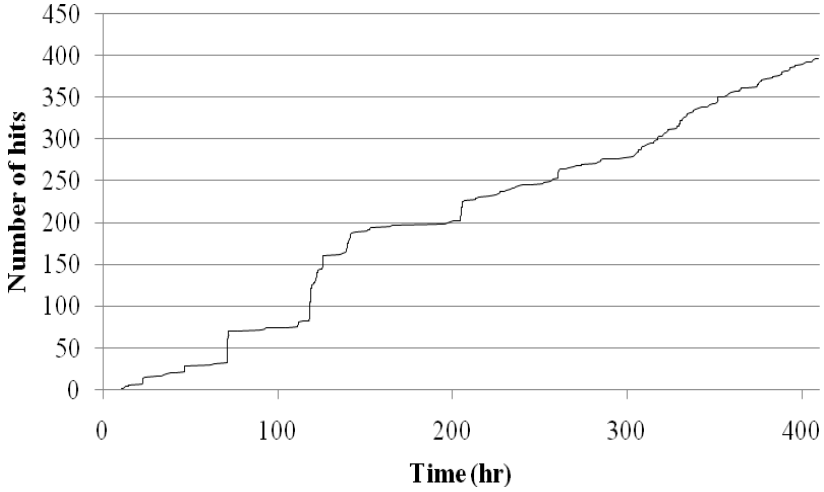

Figure 3: Number of collected hits versus test times of sample S3-1

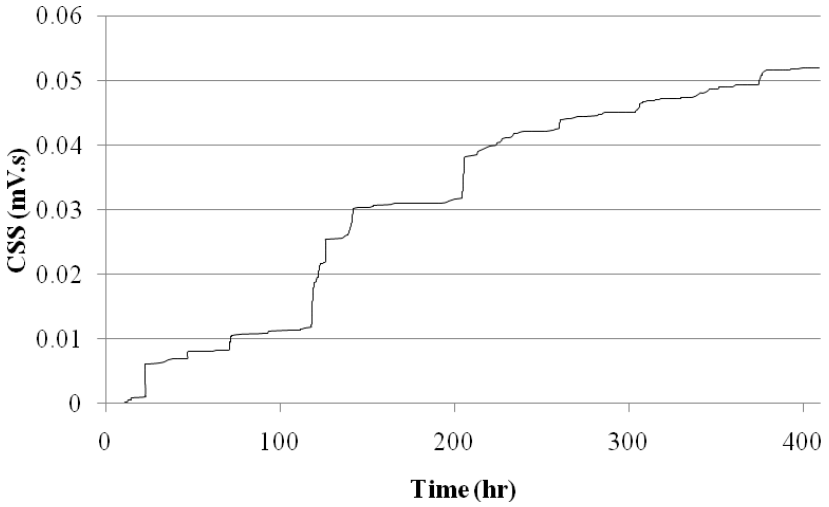

Figure 4: Cumulative signal strength (CSS) versus test time of sample S3-1

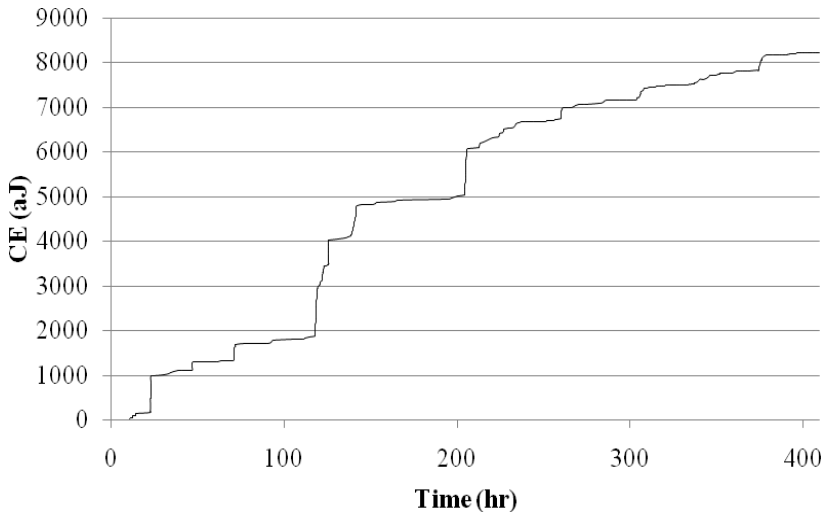

Figure 5: Cumulative energy (CE) versus test time of sample S3-1

3.3 Evaluation of Cover Cracking Using AE Intensity Analysis

The signal strength values were further analyzed to quantify the cover crack growth in all tested samples of different corrosion levels. Thus, an intensity analysis on the signal strength values of all acquired signals of each tested sample was completed to obtain two parameters: historic index (*H (t)*) and severity (S_r). *H (t)* indicates the sudden changes of the CSS curve slope by comparing the average signal strength of the last K hits with the average value of the signal strength of all acquired signals. The historic index was calculated based on Eq. 2 at all times of the test in all tested samples (Mangual et al. 2013, ElBatanouny et al. 2014, Vélez et al. 2015).

$$H(t) = \frac{\sum_{i=N-K+1}^{N} \frac{S_{oi}}{K}}{\sum_{i=1}^{N} \frac{S_{oi}}{N}} \quad [2]$$

Where: N = the number of hits up to time (t); and S_{oi} = signal strength of the i^{th} event (Mangual et al. 2013, ElBatanouny et al. 2014, Vélez et al. 2015).

S_r compares the average signal strength of the preceding J events with the maximum algebraic value of signal strength at any time and can be calculated using Eq. 3 (Mangual et al. 2013, ElBatanouny et al. 2014, Vélez et al. 2015).

$$[3] \qquad S_r = \sum_{i=1}^{J} \frac{S_{oi}}{J}$$

The magnitudes of the constants K in Eq. 2 and J in Eq. 3 may vary based on the type of phenomenon, degradation mechanisms, and simulation method (For instance: natural versus accelerated corrosion). As a result, parametric analysis can be performed to better understand the influence of these constants on severity and historic index based on the mechanism of damage (Vélez et al. 2015). These constants have been selected as K = 25 and J = 35 based on reviewing similar research studies for corrosion detection in concrete structures (Mangual et al. 2013, ElBatanouny et al. 2014, Vélez et al. 2015). The values of both historic index and severity were calculated continuously throughout the test for all samples using Eq. 2 and 3. For example, Figure 6 compares the values of *H (t)* and S_r of sample S3-1 corresponding to the cover crack growing. In addition, the values of *H (t)* and S_r of all tested samples at the end of corrosion exposure are included in Table 4.

Table 4: Results of number of hits, CSS, CE, amplitude, peak frequency, *H (t)*, and S_r of all tested samples at the end of tests

Specimen	Number of hits	Cumulative energy (aJ)	Cumulative signal strength (mVs)	Amplitude * (dB)	Peak frequency * (kHz)	*H (t)*	S_r (x10^6) pV.s
S1-1	117	5390	0.034	77	103	5.25	1.87
S1-2	97	3711	0.023	82	103	4.99	1.55
S2-1	154	6825	0.048	83	102	5.22	1.67
S2-2	223	6177	0.043	85	103	5.69	1.81
S3-1	397	8223	0.052	85	107	6.34	2.15
S3-2	356	7059	0.049	83	107	6.88	2.36
S4-1	510	9857	0.071	84	103	7.04	2.25
S4-2	490	8856	0.069	83	102	7.33	2.12
S5-1	538	10080	0.076	83	110	7.07	2.37
S5-2	597	11817	0.082	84	108	7.91	2.49

* The values of amplitude and peak frequency represent the maximum value of all detected signals in each sample

The results in Figure 6a indicate that increasing the crack width (after being visually detected) yielded an almost linear increase in the values of *H (t)*. It is also clear that the values of historic index did not significantly increase after the first crack detection. The values of historic index showed an increase of only 21% due to the crack growth from 0.08 to 0.72 in sample S3-1. These results indicate that most of the recorded AE activity occurred at the stages of bar expansion due to corrosion products as well as the micro-cracking of the surrounding concrete. This finding may also be attributed to the wave attenuation that may be due to the crack opening. Similarly, Figure 6b follows an overall increasing trend of the values of severity due to the increase in crack widths. For instance, sample S3-1 witnessed an increase of 28% of the original value recorded upon detection of the first visual crack. It is also obvious that the values of severity did not see a sharp increase after the formation of the first visual cover crack. These results once more indicate that most of the acquired AE signals were related to the early stages of damage at the beginning of visual cover cracking. It is worth noting that other tested samples were corroded to different levels of steel mass loss, yet they showed similar behaviour to the sample presented in Figure 6.

a)

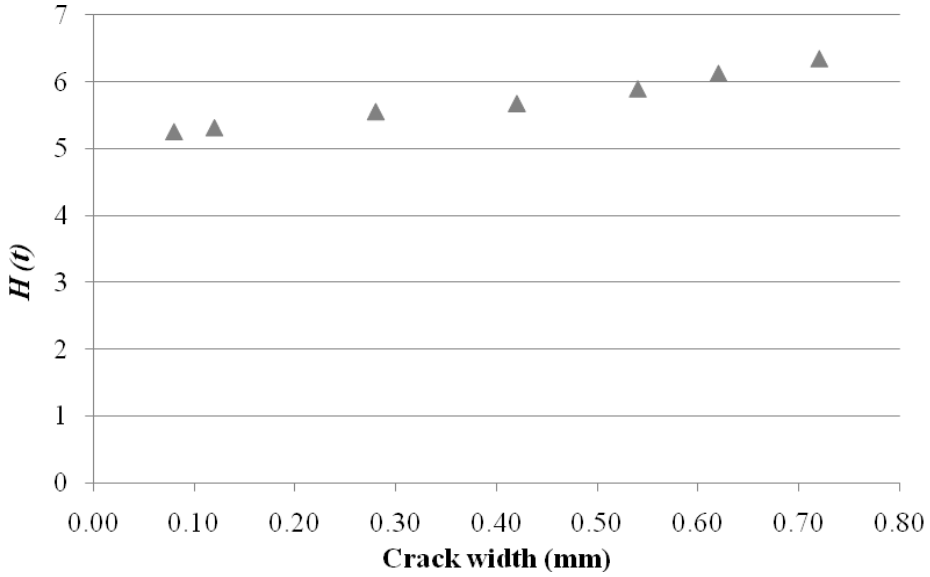

b)

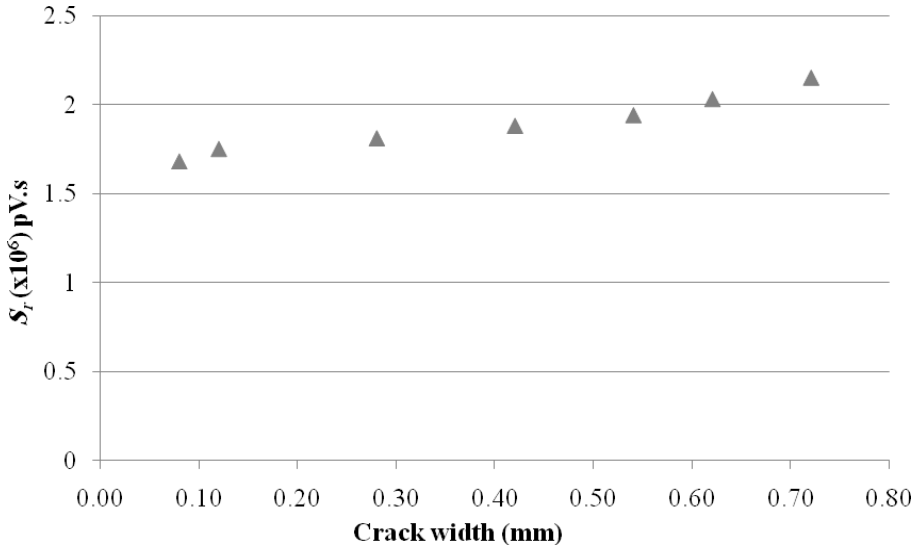

Figure 6: Intensity analysis parameters versus crack width in sample S3-1: a) *H (t)* and b) S_r

3.4 Estimation of Cover Crack Width Using AE Intensity Analysis

The results of crack widths and their corresponding values of *H (t)* and S_r for all tested specimens were used to develop an intensity classification chart (Figure 7). This chart is based on the results of cover cracking (ranging from 0.08 to 1.95 mm) in reinforced concrete samples with constant cover thickness (40 mm) due to corrosion of embedded steel. It can be utilized to correlate the different values of historic index and severity calculated based on collecting AE signal strength with the extent of damage in reinforced concrete. These kinds of damage classification charts can be suitable for the assessment of cover cracking in existing concrete structures. It should, however, be mentioned that further investigations are needed to validate the results in this chart using data collected from actual existing structures, which are exposed to natural deterioration in the form of corrosion of reinforcing steel.

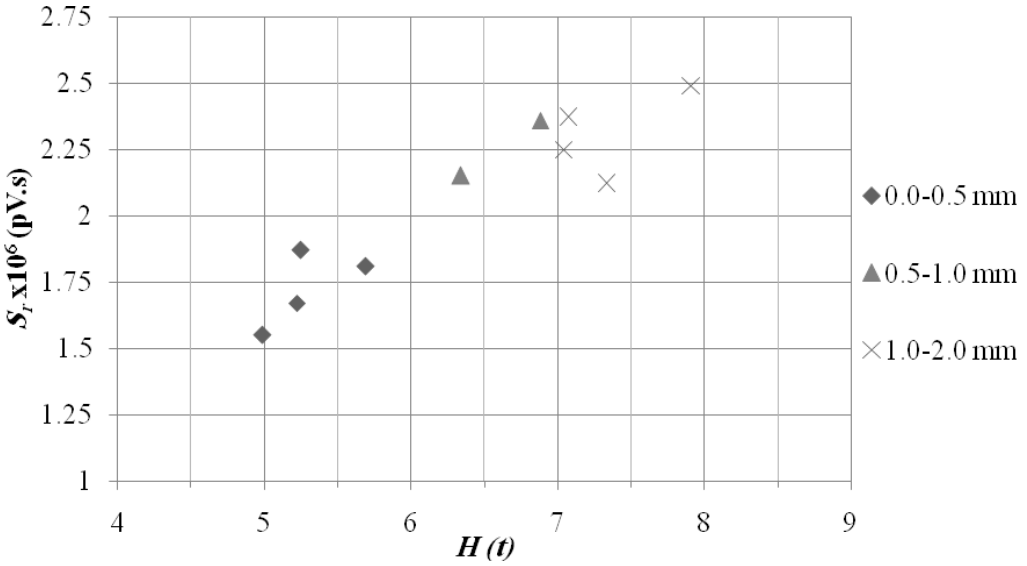

Figure 7: Cover crack width classification chart based on the results of the *H (t)* and S_r for all tested samples

4. CONCLUSIONS

Acoustic emission monitoring was applied in this experimental investigation to quantify the growth of concrete cover cracking in concrete structures due to reinforcing steel corrosion. Small-scale reinforced concrete prism samples were subjected to accelerated corrosion conditions to induce cover cracking. The samples were exposed to accelerated corrosion to reach different levels of steel mass loss (1%, 2%, 3%, 4%, and 5%). The acquired AE signals in all specimens were analyzed and then further incorporated in an intensity analysis to evaluate the extent of damage in all tested samples. The following conclusions were drawn from the analysis of results described in this paper:

- The growth of crack width due to corrosion propagation showed a significant impact on different AE parameters. This growth in crack widths resulted in an overall increase in the results of number of hits, cumulative signal strength (CSS), and cumulative energy (CE) in all tested samples regardless of the corrosion level (percentage of steel mass loss). The variation of these parameters with respect to the test time showed a similar increasing trend in all tested samples.
- The increase of crack widths also yielded an overall rise in the magnitudes of intensity analysis parameters (*H (t)* and S_r) at all corrosion levels.
- The results indicated that the most of the recorded AE activity (in terms of the values of *H (t)* and S_r) was associated with the stages of bar expansion because of corrosion products followed by the micro-cracking of the surrounding concrete prior to the first crack detection.
- The intensity analysis parameters (*H (t)* and S_r) at the same crack widths showed very similar values at all percentages of steel mass loss. The results of the intensity analysis parameters corresponding to crack widths of all tested specimens (ranging from 0.08 to 1.95 mm) were employed to develop an intensity classification chart. This chart can be utilized to assess the cover crack widths as a function of the collected AE signal strengths resulting from corrosion damage in concrete structures.

REFERENCES

Di Benedetti, M., Loreto, G., Matta, F. and Nanni, A. 2013. Acoustic Emission Monitoring of Reinforced Concrete under Accelerated Corrosion. *Journal of Materials in Civil Engineering*, 25: 1022-1029.

ElBatanouny, M. K., Mangual, J., Ziehl, P. H. and Matta, F. 2014. Early Corrosion Detection in Prestressed Concrete Girders Using Acoustic Emission. *Journal of Materials in Civil Engineering*, 26: 504-511.

Kawasaki, Y., Wasad, S., Okamoto, T. and Izuno, K. 2014. Evaluation for RC Specimen Damaged from Rebar Corrosion by Acoustic Emission Technique. *Construction and Building Materials*, 67: 157-164.

Li, Z., Zdunek, A., Landis, E. and Shah, S. 1998. Application of Acoustic Emission Technique to Detection of Reinforcing Steel Corrosion in Concrete. *ACI Materials Journal*, 95(1): 68-76.

Mangual, J., ElBatanouny, M., Ziehl, P. and Matta, F. 2013. Acoustic-Emission-Based Characterization of Corrosion Damage in Cracked Concrete with Prestressing Strand. *ACI Materials Journal*, 110(1): 89-98.

Mistras Group (2007) PCI-2 based AE system 1 user's manual. Physical Acoustics Corporation, Princeton Junction, NJ, USA.

Nair, A. and Cai, C. S. 2010. Acoustic Emission Monitoring of Bridges: Review and Case Studies. *Engineering Structures*, 32(6): 1704-1714.

Oh, B., Kim, K. and Jang, B. 2009. Critical Corrosion Amount to Cause Cracking of Reinforced Concrete Structures. *ACI Materials Journal*, 106(4): 333-339.

Ohtsu, M. and Tomoda, Y. 2008. Phenomenological Model of Corrosion Process in Reinforced Concrete Identified by Acoustic Emission. *ACI Materials Journal*, 105(2): 194-199.

Otieno, M. B., Alexander, M. G. and Beushausen, H. D. 2010. Corrosion in Cracked and Uncracked Concrete: Influence of Crack Width, Concrete Quality and Crack Reopening. *Magazine of Concrete Research*, 62(6): 393-404.

Physical Acoustics (2005) R6I-AST sensor. Princeton Junction, NJ, USA.

Ramadan, S., Gaillet, L., Tessier, C. and Idrissi, H. (2008) Detection of Stress Corrosion Cracking of High-Strength Steel Used in Prestressed Concrete Structures by Acoustic Emission Technique. *Applied Surface Science*, 254: 2255-2261.

Vélez, W., Matta, F. and Ziehl, P. 2015. Acoustic Emission Monitoring of Early Corrosion in Prestressed Concrete Piles. *Structural Control and Health Monitoring*, 22: 873-887.